DELPHI Collaboration DELPHI 2005-011 CONF 731
31 May, 2005

A Study of Excited b-Hadron States with the DELPHI Detector at LEP

Z. Albrecht, G. Barker, M. Feindt, U. Kerzel, M. Moch
Institüt fur Experimentelle Kernphysik, Universität Karlsruhe, Karlsruhe (Germany).
P. Kluit
NIKHEF, Amsterdam (The Netherlands).

Abstract

New analyses from DELPHI on the spectroscopy of excited b-hadron states, using data collected during the years 1992-2000, are reported. The total $\mathrm{B}^{**}_{\mathrm{u,d}}$ production rate,

$$\frac{\sigma(\mathrm{B}^{**}_{\mathrm{u,d}}) \cdot \mathrm{BR}(\mathrm{B}^{**}_{\mathrm{u,d}} \to \mathrm{B}^{(*)}\pi)}{\sigma_{\mathrm{b}}} = 0.156 \pm 0.011(\mathrm{stat.})^{+0.022}_{-0.014}(\mathrm{syst.}) \pm 0.019(\mathrm{model})$$

the narrow $\mathrm{B}^{**}_{\mathrm{u,d}}$ production rate,

$$\left(\frac{\sigma(\mathrm{B}^{**}_{\mathrm{u,d}}) \cdot \mathrm{BR}(\mathrm{B}^{**}_{\mathrm{u,d}} \to \mathrm{B}^{(*)}\pi)}{\sigma_{\mathrm{b}}}\right)_{\mathrm{narrow}} = 0.091 \pm 0.007^{+0.013}_{-0.008} \pm 0.011,$$

and the masses of the narrow states B^*_2 and B_1,

$$m(\mathrm{B}^*_2) = 5738 \pm 14\ \mathrm{MeV/c}^2,\ m(\mathrm{B}_1) = 5732 \pm 20\ \mathrm{MeV/c}^2,$$

have been measured.

For $\mathrm{B}^{**}_{\mathrm{s}}$ mesons, only one narrow peak can be observed which is interpreted as originating from the decay $\mathrm{B}^*_{s2} \to \mathrm{BK}$. The corresponding production rate:

$$\frac{\sigma(\mathrm{B}^*_{\mathrm{s2}}) \cdot \mathrm{BR}(\mathrm{B}^*_{\mathrm{s2}} \to \mathrm{BK})}{\sigma_{\mathrm{b}}} = 0.0093 \pm 0.0020 \pm 0.0013,$$

and the B^*_{s2} mass:

$$m(\mathrm{B}^*_{s2}) = 5852 \pm 5\ \mathrm{MeV/c}^2.$$

have been measured.

A search has been made for $\Sigma_{\mathrm{b}}^{(*)}$ baryons. No narrow signal was observed, and an upper limit on the production fraction of a single narrow state has been set:

$$\frac{\sigma(\Sigma_{\mathrm{b}}^{(*)}) \cdot \mathrm{BR}(\Sigma_{\mathrm{b}}^{(*)} \to \Lambda_{\mathrm{b}}\pi)}{\sigma_{\mathrm{b}}} < 0.012 \text{ at } 95\%\mathrm{C.L.}$$

Contributed Paper for LP 2005 (Uppsala) and HEP-EPS 2005 (Lisbon)

1 Introduction

A primary motivation for studying excited B states is to test the predictions of non-perturbative models based on the Heavy Quark Effective Theory (HQET) and thus make progress in understanding the nature of the QCD potential. Heavy quark systems are appropriate for this as they can be considered as the QCD equivalent of the hydrogen atom. A further argument comes from the observation that a large production rate of excited states would be useful in tagging the b quark flavour (i.e. b or $\bar{\mathrm{b}}$) of a b hadron at the time of its production. This is important for B^0 oscillation and CP violation studies at high energy colliders.

The motivation to reanalyse the Z data for excited B states is threefold. The new analyses profit from the improved understanding of the data, and from the development of new discriminating variables and neural networks. Secondly, the experimental results in the charm sector have been improved recently and allow a more detailed and consistent extraction of expected masses and production rates in the B sector that could be compared with measurements. Thirdly, the experimental results for the excited B production rates are rather scattered and suffer from a large systematic error coming from the combinatorial background situated under the studied signals which was, in most cases, taken from the simulation. It was found that this background was not well described by the simulation and therefore two approaches were followed which aim at reducing this source of systematics: (a) by fitting as much of the background shape as possible from data (the *High Efficiency Analysis or HEA*) or (b) by reducing the combinatorial background level (the *High Purity Analysis or HPA*).

This paper reports on a search for orbitally excited, i.e. $L = 1$, B mesons and $\Sigma_{\mathrm{b}}^{(*)}$ baryons in $\mathrm{Z} \to \mathrm{b}\bar{\mathrm{b}}$ events registered in the years 1992 to 1998 by the DELPHI experiment. The data taken in 1996 to 1998 were calibration runs. Searches are made in the channels:

$$\begin{aligned} \mathrm{B}_{\mathrm{u}}^{+**} &\to \mathrm{B}^{(*)0}\pi^+ \\ \mathrm{B}_{\mathrm{d}}^{0**} &\to \mathrm{B}^{(*)+}\pi^- \\ \mathrm{B}_{\mathrm{s}}^{0**} &\to \mathrm{B}^{(*)+}\mathrm{K}^- \\ \Sigma_{\mathrm{b}}^{(*)\pm} &\to \Lambda_{\mathrm{b}}^0\pi^\pm \end{aligned}$$

and their charge conjugated states. Throughout this paper we will refer to the meson states, generically, as B^{**}.

An overview of theoretical expectations and current results on B^{**} spectroscopy and a brief description of the DELPHI detector are given in Sections 2 and 3 respectively. General features of the two analyses developed to study $\mathrm{B}_{\mathrm{u,d}}^{**}$ are given in Section 4. The paper subsequently discusses the experimental results for the $\mathrm{B}_{\mathrm{u,d}}^{**}$ analyses (Section 5), the $\mathrm{B}_{\mathrm{s}}^{**}$ analysis (Section 6) and the search for $\Sigma_{\mathrm{b}}^{(*)}$ baryons (Section 7).

2 Current Status

2.1 Theoretical Expectations

Central to theoretical predictions in the spectroscopy of b-hadron states is the use of an approximate heavy flavour symmetry that exists because the mass of the b quark is large relative to the value of Λ_{QCD}. The symmetry is only exact in the heavy quark mass limit $m_{\mathrm{b}} \to \infty$. In the resulting theoretical framework of the Heavy Quark Effective Theory (HQET) [1], the spin of the b quark ($\vec{S}_b$) in a hadron is decoupled from the total

J_q	J^P	B^{**} state	Decay Mode	Width
1/2	0^+	B_0^*	$B\pi$	Broad ($L_p = 0$, S-wave)
1/2	1^+	B_1^*	$B^*\pi$	Broad ($L_p = 0$, S-wave)
3/2	1^+	B_1	$B^*\pi$	Narrow ($L_p = 2$, D-wave)
3/2	2^+	B_2^*	$B^*\pi, B\pi$	Narrow ($L_p = 2$, D-wave)

Table 1: *Properties of the four* $B_{u,d}^{**}$ *states.*

angular momentum of the light spectator system ($\vec{J_q} = \vec{S_q} \oplus \vec{L}$). Each energy level of the $b\bar{q}$-system thus consists of a pair of states labelled by J_q and the *total spin* $\vec{J} = \vec{J_q} \oplus \vec{S_b}$, i.e. by $J = J_q \pm 1/2$. In the heavy quark limit the two states are degenerate in mass and have the same width.

For orbitally excited states with $L = 1$, combining $J_q = 1/2$ and $3/2$ with $S_b = \pm 1/2$ gives *four* B^{**} meson states with $J^P = 0^+,\ 1^+,\ 1^+$ and 2^+. Parity conservation limits the orbital angular momentum (L_p), present in their 2-body decay modes, to be even valued. Excluding multi-pion decay channels leads to the decay modes listed in Table 1 for the $B_{u,d}^{**}$ states. A similar pattern is expected for B_s^{**} states although, isospin conservation demands that - if the B_s^{**} mass is above threshold - these states decay to $B^{(*)}K$.

Members of the $J_q = 3/2$ doublet are expected to be narrow, since only $L_p = 2$ (D-wave) transitions are allowed. The other states can decay in an S-wave and are expected to be broad. The broad state with $J = 1$ is denoted as B_1^* throughout the paper in order not to get confused with the corresponding narrow state, although the proper notation is also B_1.

Within a doublet the mass degeneracy of the two states is expected to be broken by hyperfine splitting. Various models (e.g. [2]- [12]) predict that the mass difference between the two states within the $J_q = 1/2$ and $J_q = 3/2$ doublets, should be approximately the same and in the range of $5 - 20$ MeV/c^2.

Models do not agree on the hierarchy between mass central values of the two doublets. Some models [4,5] predict that broad $B_{u,d}^{**}$ states should be lower in mass than the narrow ones with a splitting between the B_1^* and the B_1 states of about 10 MeV/c^2. Others [6,7] predict a 'spin-orbit inversion' effect where broad states are higher in mass than the narrow states. In these models the B_1^* has a mass which can be up to 150 MeV/c^2 higher than the B_1 mass.

The widths of the broad states are expected to lie between 200 and 300 MeV/c^2 [3,6].

Properties of orbitally excited charm mesons are expected to follow the same pattern with corrections to the heavy quark limit being in the ratio of the c and the b quark masses, m_b/m_c, i.e. approximately three [1, 7, 8]. This scaling is expected to apply for all mass splittings which cancel in the heavy quark mass limit. It is well verified for the doublets comprising the 0^- and 1^- states: $m_{B^*} - m_B \simeq (m_{D^*} - m_D)/3$.

Production rates of hadrons in jets depend on their mass and spin values. Neglecting mass effects, vector states are expected to be produced, promptly, three times more than pseudo-scalar mesons. This has been well verified for B^* and B mesons which have similar masses. Mass effects are already visible for the D^*-D system. As present measurements cannot determine production fractions of the different B^{**} states, two extreme scenarios have been considered and observed differences in the measured quantities have been included in the systematics. Counting the available spin states predicts the production ratios $B_2^* : B_1 : B_1^* : B_0^*$ to be $5 : 3 : 3 : 1$, whereas state counting predicts a similar production rate for all states.

2.2 Experimental Status

2.2.1 Results in the Charm Sector

The narrow $\mathrm{D}^{**}_{\mathrm{u,d}}$ and $\mathrm{D}^{**}_{\mathrm{s}}$ states are well established [13]. For broad states, progress has been made recently. CLEO has presented a signal of the broad state D^*_1 in the mass region of the narrow resonances [14]. BELLE [15] has confirmed this result and provided evidence for the other broad state, the D^*_0, lying approximately 150 MeV/c^2 lower in mass.

BABAR and CLEO [16] have shown evidence for two narrow states lying below the DK-threshold and decaying into $\mathrm{D}^{+(*)}_{\mathrm{s}}\pi^0$. These particles could be the broad $\mathrm{D}^{+*}_{\mathrm{s0}}$ and $\mathrm{D}^{+*}_{\mathrm{s1}}$ states. An overview of the mass and width measurements for D^{**} states is given in Table 2. They do not support the idea of spin-orbit inversion in the charm sector.

	Meson	Mass [MeV/c^2]	Width [MeV/c^2]
World Av.	D^0_2	2458.9 ± 2.0	23 ± 5
World Av.	D^+_2	2459 ± 4	25^{+8}_{-7}
World Av.	D^0_1	2422.2 ± 1.8	$18.9^{+4.6}_{-3.5}$
World Av.	D^+_1	2427 ± 5	28 ± 8
CLEO	D^{0*}_1	2461 ± 50	290 ± 100
BELLE	D^{0*}_1	2427 ± 36	384 ± 117
BELLE	D^{0*}_0	2308 ± 36	276 ± 66
World Av.	$\mathrm{D}^+_{\mathrm{sJ}}$	2572.4 ± 1.5	15^{+5}_{-4}
World Av.	$\mathrm{D}^+_{\mathrm{s1}}$	2535.3 ± 0.3	< 2.3
CLEO	$\mathrm{D}^*_{\mathrm{sJ}}(2460)$	2458.8 ± 1.0	< 5
BABAR	$\mathrm{D}^*_{\mathrm{sJ}}(2317)$	2317.4 ± 0.6	< 5

Table 2: *Current world results for the mass and width of* D^{**} *states. For the orbitally excited* $\mathrm{D_s}$ *states the notation* $\mathrm{D_{sJ}}$ *is used since the value for the quantum number* J *is not yet established.*

There are also measurements [13,15,17] of the relative branching ratio, $\Gamma(\mathrm{D}\pi)/\Gamma(\mathrm{D}^*\pi)$, for neutral and charged D^*_2 mesons (see Table 3). These results are compatible with the spread of values (1.5-3), expected from theory [3, 8]. For the $\mathrm{D}^*_{\mathrm{s2}}$, only a limit exists: $\Gamma(\mathrm{D}^{0*}\mathrm{K}^+)/\Gamma(\mathrm{D}^0\mathrm{K}^+) < 0.33$ [18].

	Meson	$\Gamma(\mathrm{D}\pi)/\Gamma(\mathrm{D}^*\pi)$
World Av.	D^{*0}_2	2.3 ± 0.6
BELLE	D^{*0}_2	1.9 ± 0.5
CLEO	D^{*+}_2	$1.9 \pm 1.1(\mathrm{stat.}) \pm 0.3(\mathrm{syst.})$

Table 3: *Current results for relative branching ratios of* D^*_2 *mesons into* $D\pi$ *and* $D^*\pi$*. The world average [13] has been obtained without including the BELLE measurement.*

2.2.2 Implications for the Beauty Sector

Using results listed in Table 2, and applying the m_c/m_b scaling on the mass splitting within the doublets (see Section 2.1), the corresponding mass difference in the beauty sector can be predicted. A value of about 12 MeV/c^2 for the mass difference within the narrow doublets is expected, whereas the splitting within broad doublets is of the order of 45 MeV/c^2. Similar values are obtained for non-strange and strange mesons.

Measured branching fractions of the D_2^* meson can also be used to make a prediction for the branching fractions of the B_2^* into $B\pi$ and $B^*\pi$ final states. These decay modes occur in a D-wave, leading to the following relations:

$$\Gamma(D_2^* \to D\pi)/\Gamma(D_2^* \to D^*\pi) = F_c \left(\frac{k_D}{k_{D^*}}\right)^5 \quad (1)$$

$$\Gamma(B_2^* \to B\pi)/\Gamma(B_2^* \to B^*\pi) = F_b \left(\frac{k_B}{k_{B^*}}\right)^5, \quad (2)$$

where k_D and k_{D^*} denote the momentum of the pion in the rest frame of the D_2^* in the decay $D_2^* \to D\pi$ and $D_2^* \to D^*\pi$ respectively and analogously for the B case. $F_{c,b}$ denote the ratios between the form factors in the two decay channels. Using heavy quark symmetry for the D_2^* and B_2^* states [3], it will be assumed that $F_b = F_c$. With $k_B =$ 412 MeV/c, $k_{B^*} = 367$ MeV/c (using a B_2^* mass of 5730 MeV/c^2) and $F_c = 0.61 \pm 0.16$, this gives $\Gamma(B_2^* \to B\pi)/\Gamma(B_2^* \to B^*\pi) = 1.1 \pm 0.3$

Results from BABAR and CLEO [16], on strange charm excited mesons (see Section 2.2.1), give an indication that broad B_s^{**} states can lie below the BK-threshold.

2.2.3 Results in the Beauty Sector

Evidence for narrow $B_{u,d}^{**}$ states first emerged in analyses at LEP in 1995 in which a charged pion produced at the primary event vertex was combined with an inclusively reconstructed B meson [19]- [21]. Then, the ALEPH Collaboration performed an analysis combining a primary charged pion with a fully reconstructed B meson [22] and measured the mass and rate in a fit to the mass spectrum using fixed mass differences, widths and relative rates for all spin states according to the predictions of [10]. Subsequently the L3 Collaboration reported in 1999 an inclusive measurement of the mass and width of B_1^* and B_2^* states using a fit in which constraints are applied that reflect the level of understanding regarding the widths and masses of B^{**} states at that time [23]. In 2001 OPAL studied the branching fraction of excited B states into $B^*\pi$ [24]. More recently, the CDF experiment has presented first results on $B_{u,d}^{**}$ production at a hadron collider [25] by combining a charged primary pion with a partially reconstructed B meson in semileptonic decays.

Table 4 summarises measurements of $B_{u,d}^{**}$ states. To enable a comparison, published numbers have been adjusted, where possible, to be valid for a common set of input parameters. Note that it is difficult to make a precise comparison between the results, because the fraction of broad states included in the observed signal is not known.

Experimental evidence for the B_s^{**} meson is less compelling than for $B_{u,d}^{**}$ and, to date, OPAL [19] is the only collaboration reporting a significant signal. They observed an excess over background of 149 ± 31 B^+K^- pairs (with invariant mass 5853 ± 15 MeV/c^2 and 47 ± 22 MeV/c^2 width [13]), which translates into the following production fraction:

	$m(\mathrm{B}^{**}_{\mathrm{u,d}})$ [MeV/c^2]	$\sigma(\mathrm{B}^{**}_{\mathrm{u,d}})/\sigma_{\mathrm{b}}$
OPAL incl.	5712 ± 11	0.21 ± 0.05
DELPHI incl.	$5732 \pm 5 \pm 20$	$0.27 \pm 0.02 \pm 0.06$
ALEPH incl. (all)	$5734 \pm 3 \pm 16$	$0.214 \pm 0.012 \pm 0.045^{+0.030}_{-0.045}$
ALEPH incl.(peak)	$5734 \pm 3 \pm 16$	$0.144 \pm 0.008 \pm 0.030$
L3 incl.	$\mathrm{B}^*_2 : 5768 \pm 5 \pm 6$	$0.32 \pm 0.03 \pm 0.06$
CDF semi-excl.	$\mathrm{B}_1 : 5710 \pm 20$	$0.22 \pm 0.05 \pm 0.02$
ALEPH excl.	$\mathrm{B}^*_2 : 5739^{+8+6}_{-11-4}$	$0.24 \pm 0.07^{+0.05}_{-0.04}$

Table 4: *Current world results for the mass and production rate of* $\mathrm{B}^{**}_{\mathrm{u,d}}$ *states. Three methods can be distinguished inclusive (inc.), exclusive (excl.) and semi-exclusive (semi-excl.). The notation (all) refers to the total number of* $B^{**}_{\mathrm{u,d}}$ *states, while (peak) refers to the fitted signal. The latter one should be compared with the measurements from the other experiments.*

$$\frac{\sigma(\mathrm{B}^{**}_{\mathrm{s}}) \cdot \mathrm{BR}(\mathrm{B}^{**}_{\mathrm{s}} \to \mathrm{B}^{(*)}\mathrm{K})}{\sigma_{\mathrm{b}}} = 0.020 \pm 0.006.$$

No experimental results currently exist on broad B^{**} states, strange or not.

Also no results on the search for $\Sigma^{(*)}_{\mathrm{b}}$ baryons have been published sofar.

Results in Table 4 show some agreement for the measured masses but there is a spread of values in rate measurements. This needs to be understood and the crucial issue here is the control of the combinatorial background contribution which forms the major source of systematic error in the inclusive measurements, listed in Table 4.

3 The DELPHI Detector

A complete overview of the DELPHI detector [26] and of its performance [27] have been given elsewhere. A brief description of the elements most relevant for the present analysis is given in the following.

Charged particle tracking was performed by the Vertex Detector (VD), the Inner Detector, the Time Projection Chamber (TPC) and the Outer Detector. A highly uniform magnetic field of 1.23 T parallel to the e^+e^- beam direction, was provided by the superconducting solenoid throughout the tracking volume. The momenta of charged particles (tracks) were reconstructed with a precision of $\sigma_p/p \leq 1.5\%$ in the polar angle region $\theta > 40°$ and for $p < 10$ GeV/c.

The VD consisted of three layers of silicon micro-strip devices with an intrinsic resolution of about 8 μm in the $R-\phi$ plane transverse to the beam line[1]. In addition, from 1994 on, the inner and outer-most layers were instrumented with double-sided devices providing coordinates of similar precision in the $R-z$ plane along the direction of the beams. For tracks with hits in all three $R\phi$ VD layers the impact parameter resolution was $\sigma^2_{R\phi} = ([61/(p\sin^{3/2}\theta)]^2 + 20^2)$ $\mu\mathrm{m}^2$ and for tracks with hits in both Rz layers $\sigma^2_{Rz} = ([67/(p\sin^{5/2}\theta)]^2 + 33^2)$ $\mu\mathrm{m}^2$.

[1]The z-axis is in the direction of the electron beam, the x-axis points to the centre of the LEP ring and the y-axis upwards. R is the radius in the xy plane, θ the polar angle relative to the z-axis and ϕ the azimuthal angle, in the xy-plane, with origin on the x-axis.

Calorimeters detected photons and neutral hadrons by the total absorption of their energy. The High-density Projection Chamber (HPC) provided electromagnetic calorimetry coverage in the polar angle region $46^\circ < \theta < 134^\circ$ giving a relative precision on the measured energy E of $\sigma_E/E = 0.32/\sqrt{E} \oplus 0.043$ (E in GeV). In addition, each HPC module worked essentially as a small TPC charting the spatial development of showers and so providing an angular resolution exceeding that of the detector granularity alone. For high energy photons the angular precisions were 1.7 mrad in the azimuthal angle ϕ and 1.0 mrad in the polar angle θ.

The Hadron Calorimeter was installed in the return yoke of the DELPHI solenoid and provided a relative precision on the measured energy of $\sigma_E/E = 1.12/\sqrt{E} \oplus 0.21$ (E in GeV).

Powerful particle identification was made possible by the combination of dE/dx information from the TPC (and to a lesser extent from the VD) with information from the Ring Imaging CHerenkov counters (RICH) in both the forward and barrel regions. The RICH devices utilized both liquid and gas radiators in order to optimize coverage across a wide momentum range: liquid was used for the momentum range from 0.7 GeV/c to 8 GeV/c and the gas radiator for the range 2.5 GeV/c to 25 GeV/c.

4 Analyses

The event selection, the enrichment techniques and the experimental and theoretical constraints used in these analyses are explained in the following.

4.1 Selection of Multihadronic Events

The data have been registered with the DELPHI detector at centre-of-mass energies around the Z pole. The event selection of the *High Efficiency Analysis* has been described in [28]. From data taken in 1992 to 1995, about 3.5 million events have been analysed.

In the *High Purity Analysis*, multihadronic Z decays are selected using the following requirements:

- at least five reconstructed charged particles with momenta greater than 0.2 GeV/c and polar angles θ in the range of $20^\circ < \theta < 160^\circ$;
- the total energy of the charged particles has to be larger than 12% of the centre-of-mass energy;
- an event is divided in two hemispheres using the thrust axis and, in each hemisphere, the charged particles energy is at least 3% of the total energy.

This selection gives 1.4 million multihadronic events for 1994 data, 0.7 million for 1995 and 0.1 million for 1996-1998.

The same selections are applied to the simulated samples. Samples of $\mathrm{Z} \to \mathrm{q\bar{q}}$ and $\mathrm{Z} \to \mathrm{b\bar{b}}$ events have been generated with Jetset 7.3 [29] with tunings optimised to DELPHI data [30] followed by a detailed simulation of the detector response.

4.2 Analysis Approach and Experimental Expectations

Signals for B^{**} mesons are obtained by reconstructing, in an inclusive way, the 4-momentum of a weakly decaying b hadron which is then combined with the 4-momentum of a pion or kaon, whose trajectory is compatible with the event main vertex. Distributions of the variable Q:

$$Q = m_{\mathrm{B}\pi(\mathrm{K})} - m_{\mathrm{B}} - m_{\pi(\mathrm{K})} \tag{3}$$

are used to measure the properties of B^{**} states.

An infinitely narrow B^{**} resonance will correspond to a Q distribution, with a typical width of about 35 MeV/c^2 at a Q value around 300 MeV/c^2. Due to the definition of the Q value, states decaying into $\mathrm{B}^{*}\pi(\mathrm{K})$ correspond to a peak displaced by the B^{*}-B mass splitting of about 46 MeV/c^2, downwards.

Thus, states, such as the 2^+, decaying into $\mathrm{B}\pi$ and $\mathrm{B}^{*}\pi$ will give two peaks separated by this difference in the Q distribution, whose intensities are proportional to the corresponding branching fractions.

A narrow states doublet is thus expected to contribute three peaks to the signal. Whether these peaks will be distinguishable experimentally depends on the mass resolution. If the hyperfine splitting is as small as models predict - and the B final state is reconstructed inclusively - the mass resolution achieved in the LEP experiments will not be sufficient to separate the $\mathrm{B}^{**}_{\mathrm{u,d}}$ final states. These states will therefore be reconstructed as a single peak, with a non-Gaussian shape reflecting the underlying structure.

For $\mathrm{B}^{**}_{\mathrm{s}}$ states the situation is different. If these states lie near the $\mathrm{B}^{(*)} - \mathrm{K}$ threshold, the experimental mass resolution is expected to be sufficient to separate the different final states. The reason for this difference comes from the fact that the experimental mass resolution is approximately proportional to the Q value. So, in this case, one expects to observe two or three (depending on the mass splitting) narrow mass peaks.

The observation of the predicted *broad* states is experimentally very challenging. High statistics samples are needed to separate a possible signal from the underlying background, that has to be modelled precisely.

4.3 Enrichment Techniques

To reduce the sensitivity to the background contribution two approaches have been developed. The first (*the High Efficiency Analysis*), consists in fitting from data as much of the combinatorial background shape as possible, and the second (*the High Purity Analysis*), in reducing the background level.

The *High Efficiency Analysis* takes the background from data by making a simultaneous fit for the signal and background distributions in samples enriched and depleted in B^{**} states. This procedure reduces significantly the uncertainty from the description of the background situated below the B^{**} peak.

The *High Purity Analysis* inclusively tags the B^{**} states by neural networks. The purity of the signal is enhanced by making successively harder cuts on the neural network output. For the $\mathrm{B}^{**}_{\mathrm{u,d}}$ analysis and $\Sigma_{\mathrm{b}}^{(*)}$ search, the background shape is taken from the simulation and corrected with a parametrisation which is left free to vary in the fit. For the $\mathrm{B}^{**}_{\mathrm{s}}$ analysis, the background is fitted on data using an analytic function.

Common to the HEA and HPA analyses is the reconstruction of the weakly decaying b hadron by using inclusive techniques. Inclusive variables have been constructed to estimate the direction, the momentum, the charge and the b flavour of the weakly decaying b hadron. Detailed descriptions of these techniques can be found in [28] (HEA) and [31] (HPA). The pion (or kaon) from a B^{**} state is selected by requiring that the track comes from the primary vertex. To get enriched or depleted samples in B^{**} states, correlations between the charge of the decay pion (kaon) and the b flavour are used. When the decay particle is a pion, particle identification is used to suppress the background from kaons and protons. In the B_s^{**} analysis, particle identification is used to select charged kaons [26, 27, 32].

The distributions of the variables used for the b flavour or b production tag and for the B vertex charge tag in the HEA are shown in Figure 1. Definitions of these variables are explained in [28].

The High Efficiency Analysis

Relatively soft cuts have been designed to produce similar background shapes in the signal-enriched and depleted B^{**} samples. These shapes can be extracted from data by fitting simultaneously the two B^{**} samples, thus reducing the dependence on Monte Carlo modelling.

The High Purity Analysis

Neural networks have been used extensively for e.g. the identification of the weakly decaying hadron (separating the charged and neutral B mesons with a B^+-Net and a B^0-Net), the assignment of a track to the primary or secondary vertex (TrackNet), the charge correlation and for the enrichment of the corresponding decay track (pion or kaon) originating from the different types of B^{**} mesons [31]. These techniques have also been used to measure the B^+ and B^0 lifetimes [33] and to inclusively tag the b quark flavour in a measurement of the b quark forward-backward asymmetry at the Z pole [34]. By applying cuts on the Neural Network output variables, the backgrounds can be reduced and a purer sample of B^{**} mesons can be selected as compared with the High Efficiency Analysis.

4.4 Experimental and Theoretical Constraints

In the analysis of $B_{u,d}^{**}$ data, some parameters used to describe signal components have been left free to vary in the fit whereas others have been fixed. Possible ranges of variations, for the latter, have been defined by scaling measurements from the charm sector according to the theoretical expectations (see Section 2.2) and are considered in the systematic uncertainty evaluations. The list of these parameters and their corresponding values are given in Table 5.

parameter	central value and variation
$Q(B_2^* \to B\pi)$	fitted
$m(B_2^*) - m(B_1)$	fitted
$m(B_1) - m(B_1^*)$	0 ± 40 MeV/c^2
$m(B_1^*) - m(B_0^*)$	45 ± 15 MeV/c^2
$\Gamma(B_2^* \to B\pi)/\Gamma(B_2^* \to B^*\pi)$	1.1 ± 0.3
$\Gamma(B_1^*) = \Gamma(B_0^*)$	250 ± 50 MeV/c^2

Table 5: *Fitted and constrained parameters introduced to describe* $B_{u,d}^{**}$ *signals.*

Further parameters and parametrisations used in the fit procedure have been considered:

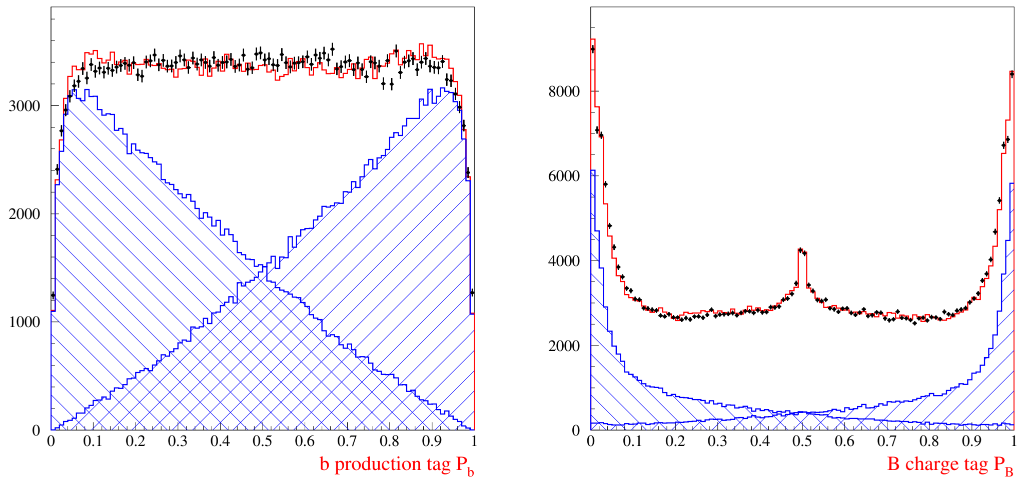

Figure 1: *Distribution for the production tag P_b (left). The dots correspond to 1992-1995 data, and the solid line to the simulation. The hatched areas correspond to the b (left) and* $\bar{\mathrm{b}}$ *(right) contributions. The udsc quarks contribution is 9% and has not been shown explicitly on the plot. Distribution for the B vertex charge tag P_B (right). The dots correspond to the 1992-1995 data, the solid lines to the simulation. The hatched areas correspond to the B^+ (left) and B^- (right) contributions. Contributions from neutral b hadrons and udsc quarks are not shown explicitly on the plot.*

• for the narrow $\mathrm{B}^{**}_{\mathrm{u,d}}$ states, three Breit-Wigner distributions are used accounting, respectively, for the two different decay modes of the B_2^* and for $\mathrm{B}_1 \to \mathrm{B}^*\pi$. The Breit-Wigner distribution is convoluted with the resolution function;

• for the mass splitting, due to the decay into B^* and B respectively, $m(\mathrm{B}^*) - \mathrm{m(B)} = 45.78 \pm 0.35\ \mathrm{MeV/c^2}$ is used [13];

• the two broad states are described by relativistic Breit-Wigner distributions;

• the relative fractions of the four $\mathrm{B}^{**}_{\mathrm{u,d}}$ states are fixed by both spin and state-counting.

In the HEA and HPA analyses a hint for a possible signal at a Q value of about 500 $\mathrm{MeV/c^2}$ is found. This enhancement (e.g. a radially excited B' state) will be called '500-state' throughout the paper. It is not interpreted as one of the two broad $\mathrm{B}^{**}_{\mathrm{u,d}}$ states, because results from the charm sector do not support spin-orbit inversion (see Section 2.2). Studies could not clarify whether this possible signal could be due to a broad resonant e.g. B' state, a wrong modelling of the fragmentation process, especially for the leading fragmentation particles or just a statistical fluctuation. Therefore, two scenarios have been considered in the fits: only narrow and broad $\mathrm{B}^{**}_{\mathrm{u,d}}$ states are fitted without and with the 500-state, parametrised as a relativistic Breit-Wigner function.

5 Results for the $\mathrm{B}^{**}_{\mathrm{u,d}}$ Analyses

In the following, the $\mathrm{B}^{**}_{\mathrm{u,d}}$ HEA and HPA analyses are both presented and then the results are combined.

5.1 The High Efficiency Analysis

Selection of $\mathrm{B}^{**}_{\mathrm{u,d}}$ events

The $\mathrm{B}^{**}_{\mathrm{d}}$ meson is selected using its decay into a B^+ and a π^-. The corresponding signature will be the presence of a $\overline{\mathrm{b}}$ quark correlated with a π^- and a charged B^+ meson, in the same event hemisphere. The $\mathrm{B}^{**}_{\mathrm{u}}$ meson is selected in its decays into a $\mathrm{B}^0_{\mathrm{d}}$ and a π^+. Here a $\bar{b}$ quark is correlated with a π^+ and a neutral $\mathrm{B}^0_{\mathrm{d}}$ meson is expected to be present in the same event hemisphere. Signals of the $\mathrm{B}^{**}_{\mathrm{d}}$ and $\mathrm{B}^{**}_{\mathrm{u}}$ mesons can therefore be separated by using the correlation between the b production tag, the B vertex charge and the charge of the pion. In the analyses, signal-enriched and depleted samples have been selected.

The event and track selection as well as the definitions of the physical quantities have been given in [28].

The following cuts have been applied to select $\mathrm{B}^{**}_{\mathrm{d}}$ candidates:
- signal-enriched sample: $q_\pi(P_b - 0.5) < 0$ and $q_\pi(P_B - 0.5) > 0.2$
- depleted sample: $q_\pi(P_b - 0.5) > 0$ and $q_\pi(P_B - 0.5) > 0.2$

where P_b denotes the b production tag probability (see Figure 1-left), P_B the B vertex charge probability (see Figure 1-right) and q_π the pion charge.

For the selection of $\mathrm{B}^{**}_{\mathrm{u}}$ candidates the following cuts have been applied:
- signal-enriched sample: $q_\pi(P_b - 0.5) > 0$ and $|(P_B - 0.5)| < 0.3$
- depleted sample: $q_\pi(P_b - 0.5) > 0$ and $q_\pi(P_B - 0.5) < -0.4$ or $q_\pi(P_b - 0.5) < 0$ and $|(P_B - 0.5)| < 0.2$

The cuts listed above have been designed to produce rather similar shapes for the $\mathrm{B}^{**}_{\mathrm{u,d}}$ background in the signal-enriched and depleted samples.

In order to become more sensitive to pions from $\mathrm{B}^{**}_{\mathrm{u,d}}$ events a weight (W_i, where the index i refers to the pion track candidate) is introduced. It exploits the fact that pions from a $\mathrm{B}^{**}_{\mathrm{u,d}}$ meson have a rather high rapidity y_i and a low probability P^B_i that they come from the secondary B vertex. This weight is defined as: $W_i = [y_i - 1.5 - 0.25 \cdot (P^B_i - 0.5)]/3$.

Q distribution parametrisation

The Q distribution for the signal-enriched sample is parametrised as:

$$S(Q) = S_{\mathrm{B}^{**}}(Q) + COR(Q) \times BKG(Q) \times (a_0 + a_1 Q + a_2 Q^2), \tag{4}$$

where $S_{\mathrm{B}^{**}}(Q)$ is the $\mathrm{B}^{**}_{\mathrm{u,d}}$ signal shape that contains several narrow and broad resonances. For one narrow resonance a sum of five Gaussian distributions is used. The signal shape is parametrised using simulated events that were generated according to a Breit-Wigner resonance with a width of 20 MeV/c^2. Five Gaussians with an r.m.s. varying from 42 to 120 MeV/c^2 were used to describe well the tails of the distribution. The total r.m.s. of a single resonance is 61 MeV/c^2 for a signal Q value of 283 MeV/c^2.

A Breit-Wigner function with a mass dependent width is taken for the broad resonance. The depleted sample parametrisation, $B(Q)$, is expressed as:

$$B(Q) = \epsilon\, S_{\mathrm{B}^{**}}(Q) + BKG(Q), \tag{5}$$

where $\epsilon(< 1)$ corresponds to the depletion of the $\mathrm{B}^{**}_{\mathrm{u,d}}$ signal in this sample relative to the enriched sample.

In the above equations, the background Q distribution -BKG- has been parametrised as:

$$BKG(Q) = THR(Q)\, b_0 e^{-b_1 Q - b_2 Q^2 - b_3 Q^3 - b_4 Q^0.5}, \tag{6}$$

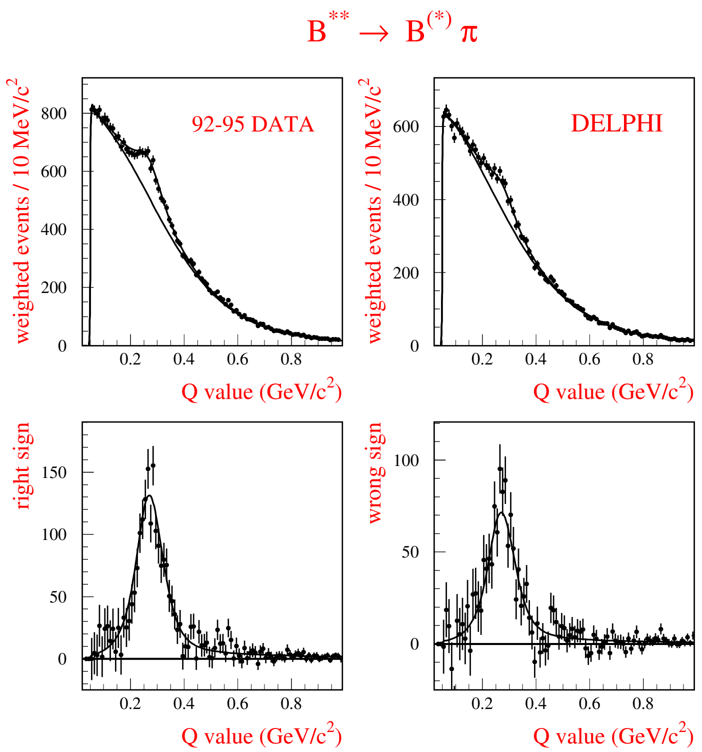

Figure 2: *The Q distributions for the $\mathrm{B}^{**}_{\mathrm{u,d}}$ signal-enriched (top left) and depleted (top right) samples. The result of the fit - assuming spin-counting and not including a possible 500-state - has been superimposed. Q distributions obtained after subtraction of the fitted background are shown in bottom plots.*

where THR is a threshold function:

$$THR(Q) = (e^{-\alpha Q} - e^{\alpha Q})/(e^{-\alpha Q} + e^{\alpha Q}) + \beta. \tag{7}$$

The ratio of the backgrounds in the signal-enriched and depleted samples $COR(Q)$ is fitted on simulated data, fixing $a_0 = 1$ and a_1 and a_2 to zero. The functional dependence is the same as in Equation (6) where b_4 is fixed to zero. The $COR(Q)$ correction is rather flat and varies by less than 3.5% over the fitted Q range. This flatness is important, because it gives confidence that the background in the signal depleted sample can be used to estimate the background under the peak in the signal-enriched sample.

It has been verified extensively on simulated events that the signal-enriched and depleted samples can be described by these functions. Of particular importance is the fact that the background in the signal-enriched sample - after fixing $COR(Q)$ - can be described by only three additional parameters a_0, a_1 and a_2, where a_1 and a_2 are small. Fits on simulated data show that a_1 and a_2 are compatible with zero within one standard deviation.

Fits to the $\mathrm{B}^{**}_{\mathrm{u,d}}$ spectra

In the fit, different scenarios for the B^{**} signal have been tested. As outlined in Section 4.4, there are two free parameters for the narrow states: the Q value of the highest mass state decaying into $\mathrm{B}\pi$, $Q(\mathrm{B}^*_2 \to \mathrm{B}\pi)$ is left free, as well as the mass splitting between the narrow B^*_2 and B_1 state.

The masses and widths of the broad states are fixed at the values listed in Section 4.4, their production rate varies according to the hypothesis of spin or state-counting. The possible 500-state is fitted adding to Equation (5) a Breit-Wigner function with a free central value Q(500-state), width Γ(500-state) and amplitude.

In the fit, the value of ϵ is fixed to 0.546 and the parameters of the threshold function are fixed at $\alpha = 200$ $(\mathrm{GeV/c^2})^{-1}$ and $\beta = 1$, as determined using simulated events. The parameters that describe the background a_0, a_1, a_2 and b_0 to b_4 are left free to vary in the fit.

The χ^2 fit is performed using the signal-enriched and depleted samples, within the range of Q values ranging from 0.05 to 1 GeV/c^2. The weighted number of events is fitted. The $\mathrm{B_d^{**}}$ and the $\mathrm{B_u^{**}}$ spectra are fitted separately. The results are compatible within their respective errors and therefore it has been decided to combine the distributions and to fit the total $\mathrm{B_{u,d}^{**}}$ spectrum. Production rates for $\mathrm{B_d^{**}}$ and $\mathrm{B_u^{**}}$ mesons are then determined. They are defined as:

$$\frac{\sigma(\mathrm{B_{u,d}^{**}}) \cdot \mathrm{BR}(\mathrm{B_{u,d}^{**}} \to \mathrm{B^{(*)}}\pi)}{\sigma_\mathrm{b}} = \frac{1}{\sigma_\mathrm{b}} \sum_{q=u,d} \sigma(\mathrm{B_q^{**}}) \left[\mathrm{BR}(\mathrm{B_q^{**}} \to \mathrm{B}\pi) + \mathrm{BR}(\mathrm{B_q^{**}} \to \mathrm{B^*}\pi)\right], \quad (8)$$

where σ_b is the b quark production cross section.

As the experiment is sensitive only to charged pion $\mathrm{B_{u,d}^{**}}$ decay modes, measured rates have been multiplied by 3/2 to correct for channels involving a π^0. The total rate and the rates for narrow states and for the 500-state are measured[2]. The fits are performed considering four scenarios: without and with fitting the 500-state, and assuming spin or state-counting for production rates of narrow and broad $\mathrm{B^{**}}$ mesons. Results are listed in Tables 6 and 7. Those obtained assuming spin-counting and not including the 500-state are shown in Figure 2. In Figure 3, the 500-state has been included in the fit.

The systematic errors are obtained by varying the Q value where the fit starts, cutting in the weights W_i distribution, and changing the signal shape and the Q or energy scale. The last systematic error comes from the uncertainty in the inclusive B energy reconstruction. The signal shape was changed taking into account descrepancies of 10% in the Q resolution between data and simulation. Changes in the first two error sources are the dominant error source for the cross-section measurement. The uncertainty in the Q scale and signal shape mainly affect the mesasured Q value and mass splitting.

There is no additional systematic error coming from background shapes (taken from the simulation), because the backgrounds are fitted on the data.

The χ^2 improvement, when adding a Breit-Wigner function to describe the 500-state, is 16. Taking into account the systematics, the evidence for a broad resonance is only about 2 standard deviations.

It is difficult to make a definite statement about state or spin-counting. The data have a slight preference for spin-counting at the level of about 1.5 standard deviations. Note that the rate of narrow plus broad states, assuming spin (state) counting, is by definition 1.5 (2) times the rate for the narrow states. In data there is only clear evidence for the existence of narrow states, the broad states are assumed to be there, as in the charm sector.

To extract results for the production rates of narrow and narrow plus broad states, measurements obtained in the scenarios without and with including the 500-state have been averaged and half the difference between the two values has been taken as a systematic error (denoted by 'scen.'). Uncertainties coming from the range of variation of the parameters (see Table 5), which have been held fixed in the fit have been also included as systematics, under the same label. The same procedure has been applied to evaluate

[2]Thus, the 'total rate' refers to narrow plus broad states (excluding the 500-state), the 'narrow rate' refers to narrow states.

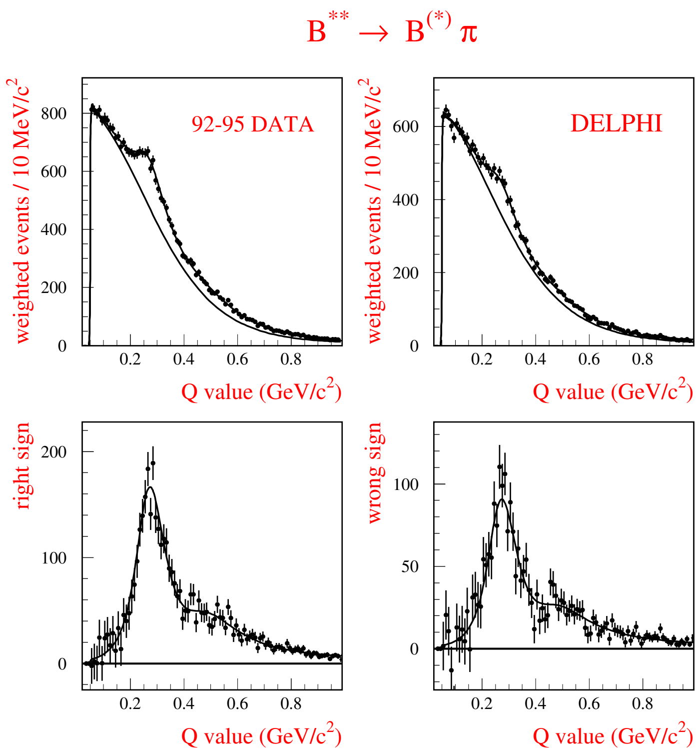

Figure 3: *The Q distributions for the* $B^{**}_{u,d}$ *signal-enriched (top left) and depleted (top right) samples. The result of the fit - assuming spin-counting and including a possible 500-state - has been superimposed. Q distributions obtained after subtraction of the fitted background are shown in bottom plots.*

the ('model') systematic uncertainty, related to the spin or state-counting scenarios. The results are listed in Table 8.

It is possible to extract from the fit a limit on the width of the narrow state signals. This was done by assuming that the mass splitting between the narrow states is zero and allowing for additional width of the signal. The signals are compatible with a width of 20 MeV/c^2 that was used in the simulation. The upper limit on the width corresponds to 40 MeV/c^2 at 95% C.L. including systematic errors.

Scenario	Counting	χ^2/ndof	Total $B^{**}_{u,d}$-rate	Narrow $B^{**}_{u,d}$-rate	$Q(B_2^* \to B\pi)$ (MeV/c^2)	$(m(B_2^*)-m(B_1))$ (MeV/c^2)
500 out	Spin	167/179	0.126±0.006±0.016	0.084±0.004±0.011	$307 \pm\ 7 \pm 12$	$-11 \pm 13 \pm 9$
	State	170/179	0.149±0.008±0.019	0.075±0.004±0.010	$308 \pm\ 8 \pm 12$	$-13 \pm 12 \pm 9$
500 in	Spin	151/176	0.163±0.014±0.021	0.108±0.009±0.014	$323 \pm\ 9 \pm 12$	$11 \pm 16 \pm 9$
	State	153/176	0.192±0.017±0.024	0.096±0.009±0.012	$326 \pm\ 12 \pm 12$	$5 \pm 18 \pm 9$

Table 6: HEA $B^{**}_{u,d}$-fit results for the different scenarios. The first error is the statistical one, the second is the systematical one. The systematics quoted are discussed in the main text. Note the Total and Narrow rate are fully correlated.

	500-state rate	Q(500-state) (MeV/c^2)	$\Gamma(500 - state)$ (MeV/c^2)
Spin	0.090±0.027(stat.)±0.043(syst.)	499±13(stat.)±30(syst.)	304± 40(stat.)± 50(syst.)
State	0.088±0.025(stat.)±0.042(syst.)	499±13(stat.)±30(syst.)	297± 38(stat.)± 50(syst.)

Table 7: HEA Fit results for the 500-state.

	Total $B^{**}_{u,d}$-rate	Narrow $B^{**}_{u,d}$-rate	$Q(B^*_2 \to B\pi)$ (MeV/c^2)	($m(B^*_2)-m(B_1)$) (MeV/c^2)
Spin	0.145±0.011(stat.) ±0.018 (syst.)±0.018(scen.)	0.096±0.007(stat.) ±0.014(syst.)±0.012(scen.)	315±8(stat.) ±12(syst)±8(scen.)	0±15(stat.) ±9(syst.)±11(scen.)
State	0.170±0.013(stat.) ±0.022(syst.)±0.022(scen.)	0.085±0.007(stat.) ±0.012(syst.)±0.011(scen.)	317±10(stat.) ±12(syst.)±9(scen.)	-4±15(stat.) ±9(syst.)±9(scen.)
Average	0.157±0.012(stat.) ±0.020(syst.)±0.025(model)	0.091±0.007(stat.) ± 0.013(syst.)±0.011(model)	316±9(stat) ±12(syst)±9(model)	-2±15(stat.) ±9(syst.)±11(model)

Table 8: HEA Averages over the two scenarios considered in Table 6. The uncertainty due to the scenarios is denoted as 'scen.' and also includes the variations due to changes in the fixed parameters (see section 4.4). Additionally the average over the two counting schemes is also given. The model error is given by the uncertainties due to the scenario and the counting scheme, added in quadrature.

5.2 The High Purity Analysis

General Event and Track Selection

An event is divided into two hemispheres using the thrust axis. A hemisphere is accepted if the following criteria are satisfied:

- the cosine of the polar angle of the thrust axis relative to the beam direction, $|\cos\theta_{thrust}|$, is less than 0.7;
- the RICH detectors and the VD are fully operational;
- the event is tagged as a $\mathrm{Z} \to \mathrm{b\bar{b}}$ event by the standard DELPHI b-tagging package [35] requiring a positive value for the btag variable;
- the secondary vertex fit from the BSAURUS package [31] has converged and
- the hemisphere energy divided by the beam energy is between 0.5 and 1.1.

These cuts select $\mathrm{b\bar{b}}$ events with a purity of 90% and an efficiency of 48%, as estimated from the simulation.

Tracks used in this analysis have to fulfill the following selection criteria:

- an impact parameter, with respect to the primary vertex in the plane orthogonal to the beam direction, of less than 4 cm;
- an impact parameter, with respect to the primary vertex in the beam direction of less than 6 cm;
- a cosine value of the polar angle, $|\cos\theta|$, of less than 0.94;
- a relative uncertainty on the momentum of the track $\frac{\Delta p}{p}$ less than 1;
- at least one $R-\phi$ hit in the vertex detector and
- not flagged as coming from a secondary interaction with the detector material [36].

Selection of $\mathrm{B}^{**}_{\mathrm{u,d}}$ Events

Neural network techniques are used extensively in the HPA with the aim of achieving high signal-to-background ratios. The main components of the analysis are:

- a Q value correction network;
- a Charge Correlation Network, based on inclusive flavour and charge tags, providing a probability that the pion candidate has the correct charge correlation to originate from a $\mathrm{B}^{**}_{\mathrm{u,d}}$ state;
- a $\mathrm{B}^{**}_{\mathrm{u,d}}$ Enhancement Network which is trained to recognize the $\mathrm{B}^{**}_{\mathrm{u,d}}$ decay pions using particle identification, track impact parameters and kinematic variables.

All networks are trained using simulated samples with $\mathrm{B}^{**}_{\mathrm{u,d}}$ states uniformly distributed in mass in order to avoid network predictions that are biased towards particular Q values. To improve the performance of the networks a set of preselection cuts is applied to the training sample, data and simulated events used in the analysis:

- the momentum of the $\mathrm{B}^{**}_{\mathrm{u,d}}$-decay pion candidate should lie between 1 and 14 GeV/c,
- the rapidity of the track w.r.t the jet axis should be greater than 1.6,
- the TrackNet output, should be lower than 0.5,
- the cosine of the helicity angle should be greater than -0.75 and
- the opening angle should be lower than 0.6 rad.

The Q value correction network is needed to correct for the bias in the reconstructed Q value. Pions from $\mathrm{B}^{**}_{\mathrm{u,d}}$ decays can be confused with decay products from the weakly decaying b hadron due for example to their relatively high rapidity. Whenever the decay

	B^{0**} r.s.	B^{+**} r.s.
B^+	71.3%	23.0%
B^0	20.0%	61.9%
B_s	2.4%	5.2%
b-baryons	2.0%	5.6%
others	4.3%	4.3%

	B^{0**}	B^{+**}
B^{**0} r.s.	1.0	0.390
B^{**0} w.s.	0.088	0.449
B^{**+} w.s.	0.136	0.374
B^{**+} r.s.	0.057	1.0

Table 9: *The composition of the right sign samples (left) and the relative fractions of $B^{**}_{u,d}$ mesons in the four samples normalised to the number of $B^{**}_{u,d}$ mesons in the corresponding right-sign samples (right), as determined by simulation.*

pion from the $B^{**}_{u,d}$ state is included in the definition of the weakly decaying state, a bias in the reconstructed Q value is introduced. This bias is removed by training a network to reproduce the correction factor $\Delta Q = Q_{rec} - Q_{true}$ using the methods described in [37].

The discrimination between B^{**0}_d (B^{**+}_u) is done by enhancing B^+ (B^0) via the B^+-Net (B^0-Net), mentioned in Section 4.3, and in the same time depleting B^0 (B^+) with an anti-cut on the appropriate network output. By imposing the following cuts on the Charge Correlation Network variable CC, a 'right-sign' (r.s.) and 'wrong-sign' (w.s.) sample for B^{**+}_u and B^{**0}_d mesons have been defined as follows:

$$
\begin{array}{llll}
1) & CC > 0.0, & B^{**0}_d \to B^+\pi^-, & \text{`right} - \text{sign'} \\
2) & CC < 0.0, & B^{**0}_d \to B^+\pi^+, & \text{`wrong} - \text{sign'} \\
3) & CC > 0.3, & B^{**+}_u \to B^0\pi^-, & \text{`wrong} - \text{sign'} \\
4) & CC < -0.3, & B^{**+}_u \to B^0\pi^+, & \text{`right} - \text{sign'}.
\end{array}
$$

where for 1) and 2) B^+ are enhanced with B^+-Net>0.4 and B^0-Net<0.4, while for 3) and 4) B^0 are enhanced with B^0-Net>0.4 and B^+-Net<0.4.

This procedure lead to a B^+ (B^0) purity of 57% (48%) in the right-sign samples as estimated by the simulation.

Additionally, a cut on the B^{**} Enhancement Network at a value of 0.3 is applied to data and simulated events respectively. The relative compositions of the r.s. samples are shown in Table 9 on the left side.

Fit to the $B^{**}_{u,d}$ Spectra

Combined fits to the four samples defined above have been performed. The background shapes $BKG(Q)_i$ in each of the four samples i = 1-4 (r.s./w.s. B^{**}_d/B^{**}_u samples) are taken from the simulation and corrected with the following cubic expression:

$$
BKG(Q)_{\mathrm{fit,i}} = BKG(Q)_{\mathrm{MC,i}} \cdot N_i \cdot (a + b \cdot Q + c \cdot Q^2 + d \cdot Q^3). \tag{9}
$$

The parameters N_i, a, b, c and d are allowed to vary freely in the fit. The parameter a can be different for the samples 1), 2) and 3), 4) respectively; parameters b, c and d are taken to be the same in all samples. Studies have revealed that the simulated background shape has to be modified to fit the data, particularly at low and high Q values. This is reflected in a substantial improvement in the fit quality and stability when the MC background shape is corrected according to the formulas described above.

The list of free parameters used in the fits to the measured Q value distribution is:

- the $B^{**}_{u,d}$ production rate;

- the mass of the B_2^*;
- the hyperfine splitting within the narrow doublet;
- the Gaussian resolution widths for B_d^{**} and B_u^{**};
- the background parameters N_i, a, b, c and d.

In all fits infinitely narrow resonances have been assumed. It has also been assumed that production rates and masses of the B_u^{**} and B_d^{**} states are equal. The mass values and relative production rates of narrow and broad states are fixed to the values discussed in Section 4.4.

Studies showed that simulated B_u^{**} data preferred a slighly higher Gaussian width (37 ± 3 MeV/c^2) than simulated B_d^{**} data (32 ± 3 MeV/c^2) for an infinitely narrow resonance at a Q value of 300 MeV/c^2. Thus, both the Gaussian widths for B_d^{**} and B_u^{**} have been fitted giving 30 ± 7 MeV/c^2 and 42 ± 8 MeV/c^2 respectively for the fit assuming spin-counting. Assuming state-counting or taking the 500-state into account makes hardly any difference to these values.

The relative fraction of $B^{0**}(B^{+**})$ mesons, expected in the fitted samples, has been fixed to the simulation values (see Table 9 on the right). The result of the fit assuming spin-counting is shown in Figure 4. If the 500-state is included in the fit, three additional free parameters are introduced: the production rate, the Q(500-state) value and the Γ(500-state). The result of the fit, including the 500-state and assuming spin-counting is shown in Figure 5.

The fits have been performed for the four scenarios considered already in the HEA, namely, without and with including the 500-state and assuming spin or state-counting. Systematic uncertainties originate from the correction applied to the background and from the $B_{u,d}^{**}$ enrichment procedures. The first uncertainty is obtained by varying the order of the polynomial, used in the correction, by $\mp$ one unit and taking the full difference of both cases as the uncertainty. This gives an asymmetric error. The uncertainty coming from the enrichment is obtained by varying the cut on the $B_{u,d}^{**}$ Enrichment Network. Systematics from the energy scale and the parameters fixed in the fit are estimated in the same way as in the HEA (see Section 5.1).

The total systematic error has been evaluated by combining in quadrature the various contributions.

Results for $B_{u,d}^{**}$ mesons are listed in Table 10 and averages, obtained using the same procedure as for the High Efficiency analysis, are given in Table 12, (see Section 5.1).

Results for the production rate of the 500-state are listed in Table 11.

5.3 Combination of the Analyses

$B_{u,d}^{**}$ averaged results, obtained by combining the HEA and the HPA, are given in Table 13. In this procedure, correlations coming from common error sources have been taken into account. The statistical overlap between the analyses is negligible. Common error sources are the energy scale and the model and scenario uncertainties.

The total $B_{u,d}^{**}$ production rate is measured to be

$$\frac{\sigma(B_{u,d}^{**}) \cdot BR(B_{u,d}^{**} \to B^{(*)}\pi)}{\sigma_b} = 0.156 \pm 0.011(\text{stat.})^{+0.022}_{-0.014}(\text{syst.}) \pm 0.019(\text{model}),$$

and the narrow $B_{u,d}^{**}$ production rate is

$$\left(\frac{\sigma(B_{u,d}^{**}) \cdot BR(B_{u,d}^{**} \to B^{(*)}\pi)}{\sigma_b}\right)_{\text{narrow}} = 0.091 \pm 0.007(\text{stat.})^{+0.013}_{-0.008}(\text{syst.}) \pm 0.011(\text{model}).$$

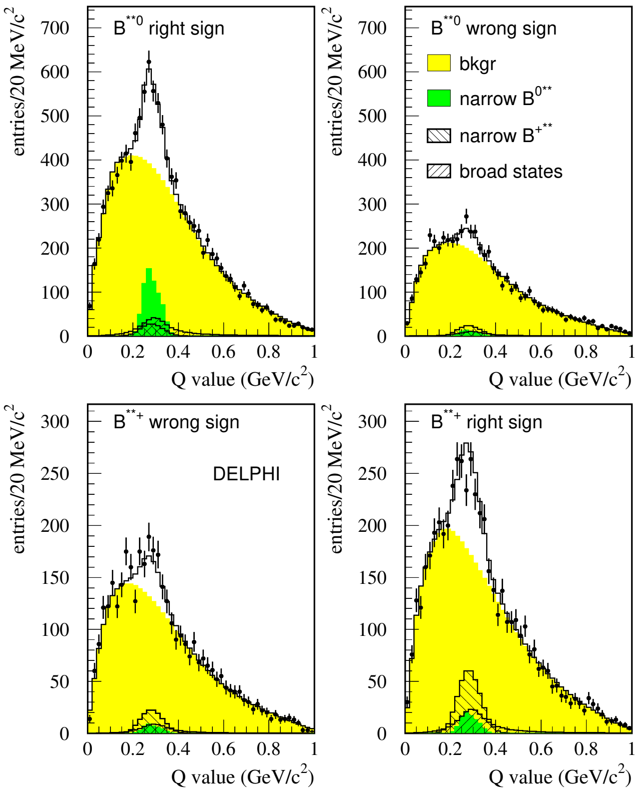

Figure 4: *Fit result for the HPA* $B^{**}_{u,d}$ *analysis without the 500-state assuming spin-counting. The points are data, the open histogram shows the fit result. The different components are explained in the figure.*

The measured Q value - of the decay $B_2^* \to B\pi$ - corresponds to a B_2^* mass of 5738 $\pm$ 14 MeV/c^2. From the measured Q value and the fitted mass splitting, the B_1 mass is determined to be 5732 $\pm$ 20 MeV/c^2.

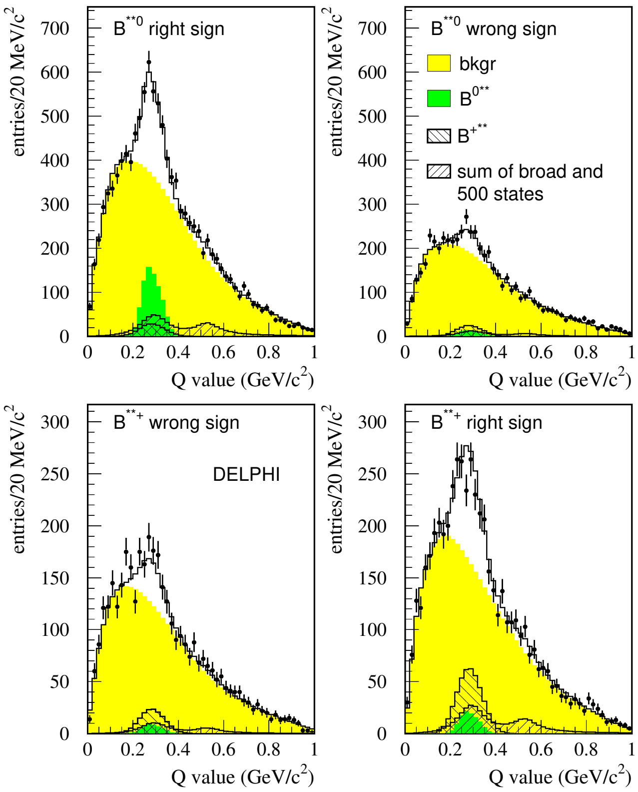

Figure 5: *Fit result for the HPA* $\mathrm{B}^{**}_{\mathrm{u,d}}$ *analysis including the 500-state assuming spin-counting. The points are data, the open histogram shows the fit result. The different components are explained in the figure.*

Scenario	Counting	χ^2/ndof	Total $B^{**}_{u,d}$-rate	Narrow $B^{**}_{u,d}$-rate	$Q(B_2^* \to B\pi)$ (MeV/c^2)	$(m(B_2^*)-m(B_1))$ (MeV/c^2)
500 out	Spin	199/186	$0.132\pm0.014^{+0.030}_{-0.008}$	$0.088\pm0.009^{+0.019}_{-0.006}$	$319 \pm 7 \pm 13$	$13 \pm 13 \pm 10$
	State	199/186	$0.150\pm0.014^{+0.027}_{-0.008}$	$0.075\pm0.007^{+0.013}_{-0.004}$	$322 \pm 11 \pm 13$	$11 \pm 15 \pm 10$
500 in	Spin	187/183	$0.153\pm0.021^{+0.055}_{-0.011}$	$0.102\pm0.014^{+0.037}_{-0.006}$	$321 \pm 8 \pm 13$	$16 \pm 14 \pm 10$
	State	187/183	$0.174\pm0.020^{+0.043}_{-0.011}$	$0.087\pm0.010^{+0.022}_{-0.006}$	$328 \pm 10 \pm 13$	$17 \pm 14 \pm 10$

Table 10: HPA $B^{**}_{u,d}$-fit results for the different scenarios. The first error is the statistical one, the second is the systematical one. The systematics quoted are due to physics effects, i.e. background correction and enrichment, only.

	500-state rate	Q(500-state) (MeV/c^2)	$\Gamma(500-state)$ (MeV/c^2)
Spin	0.030±0.014(stat.)±0.022(syst.)	531±21(stat.)±18(syst.)	260±170(stat.)±140(syst.)
State	0.031±0.018(stat.)±0.016(syst.)	532±18(stat.)±13(syst.)	250±160(stat.)±100(syst.)

Table 11: HPA fit results for the 500-state.

	Total $B^{**}_{u,d}$-rate	Narrow $B^{**}_{u,d}$-rate	$Q(B_2^* \to B\pi)$ (MeV/c^2)	$(m(B_2^*)-m(B_1))$ (MeV/c^2)
Spin	0.143±0.017(stat.) $^{+0.042}_{-0.009}$(syst.)±0.012(scen.)	0.095±0.011(stat.) $^{+0.028}_{-0.006}$(syst.)±0.008(scen.)	320±7(stat.) ±13(syst.)±9(scen.)	15±13(stat.) ±10(syst.)±5(scen.)
State	0.162±0.017(stat.) $^{+0.035}_{-0.009}$(syst.)±0.016(scen.)	0.081±0.008(stat.) $^{+0.017}_{-0.005}$(syst.)±0.008(scen.)	325±10(stat.) ±13(syst.)±9(scen.)	14±14(stat.) ±10(syst.)±6(scen.)
Average	0.153±0.017(stat.) $^{+0.038}_{-0.009}$(syst.)±0.017(model)	0.088±0.009(stat.) $^{+0.022}_{-0.005}$(syst.)±0.011(model)	323±7(stat.) ±13(syst.)±9(model)	15±13(stat.) ±10(syst.)±6(model)

Table 12: HPA averages over the two scenarios from table 10 for both spin and state counting. The uncertainty due to the scenarios is denoted as 'scen.' and also includes the variations due to changes in the fixed parameters (see section 4.4). Additionally the average over the two counting schemes is also given. The model error is given by the uncertainties due to the scenario and the counting scheme, added in quadrature.

	Total $B^{**}_{u,d}$-rate	Narrow $B^{**}_{u,d}$-rate	$Q(B_2^* \to B\pi)$ (MeV/c^2)	$(m(B_2^*)-m(B_1))$ (MeV/c^2)
Spin	0.145±0.011(stat.) $^{+0.022}_{-0.014}$(syst.)±0.014(scen.)	0.096±0.007(stat.) $^{+0.015}_{-0.009}$(syst.)±0.009(scen.)	317±5(stat.) ± 9(syst.)±9(scen.)	8±11(stat.) ± 8(syst.)±6(scen.)
State	0.167±0.011(stat.) $^{+0.022}_{-0.014}$(syst.)±0.016(scen.)	0.085±0.006(stat.) $^{+0.011}_{-0.007}$(syst.)±0.008(scen.)	321± 7(stat.) ± 9(syst.)±9(scen.)	5±11(stat.) ± 7(syst.)±6(scen.)
Average	0.156±0.011(stat.) $^{+0.022}_{-0.014}$(syst.)±0.019(model)	0.091±0.007(stat.) $^{+0.013}_{-0.008}$(syst.)±0.011(model)	319±6(stat) ± 9(syst.)±9(model)	6 ±11(stat.) ± 7(syst.)±6(model)

Table 13: Combined results for the two analyses. In the combination the errors coming from the scenario are assumed to be fully correlated.

6 A Search for B_s^{**} States

A search for B_s^{**} states, in the B^+K^- decay channel, has been made by using the approach of the HPA and by identifying the charged kaon.

Selection of B_s^{**} Events

Similar to the $B_{u,d}^{**}$ HPA, neural network techniques are used to enhance a sample in B_s^{**} decays and to correct for the bias in the measured Q value.

A B_s^{**} Enhancement Network is also constructed to identify and select B_s^{**} kaon decay candidates. The most important input variables to the network are:

- the reconstructed energy of the weakly decaying B meson;
- the probability for the weakly decaying B meson to be a charged B meson;
- for kaon candidates: the kaon signature probability, the rapidity and the probability to originate from the primary vertex;
- the decay angle of the kaon candidate in the B_s^{**} rest frame;
- the charge correlation between the B and K decay products of the B^{**}.

Adding charge correlation information to the B_s^{**} Enhancement Network, instead of defining a right- and wrong-sign sample, makes more optimal use of the information and is found to improve the overall performance of the B_s^{**} reconstruction.

Network training is performed on simulated B_s^{**} events with uniformly distributed B_s^{**} mass values in order to avoid network predictions that are biased towards a particular Q value. Since the kaon identification is crucial to the final performance of the B_s^{**} Enhancement Network, three separate networks are trained to reach kaon purities above a preselection cut value of 42%, 66% and 80% to study the dependence of the enhancement on the kaon purity. Is has been found that the Enhancement Network with a preselection cut value of 42% gave the best performance. Whenever in the following text cuts on a neural network output or stability studies are mentioned, this refers to the B_s^{**} Enhancement Network with a preselection cut value of 42%. Additionally, similar precuts as for the $B_{u,d}^{**}$ networks have been applied by replacing the pion by a kaon.

Fit to the B_s^{**} Spectrum

The signal shape is studied using simulated B_s^{**} events and parametrised using a double Gaussian distribution. Parameters of this distribution are evaluated by a fit to a simulated signal located at a Q value of 80 MeV/c^2 and having zero width. This has been done in an iterative way to identify the Q value at which the expected resolution should be determined. Typical widths of the two Gaussians are 15 and 40 MeV/c^2 respectively. The ratio of the areas of narrow to broad Gaussian is around 5:1. The widths and the ratio of the areas is fixed to the expectation in the fit.

The background shape is parametrised using the following expression [36]:

$$BKG(Q) \;=\; p_1\,[Q(p_4 - Q)]^{p_2} \cdot \exp\left[-p_3\left(Q - \frac{p_4}{2}\right)\right],$$

which contains four free parameters p_1, p_2, p_3 and p_4. This choice has been preferred instead of taking the shape from the simulation, because it is unlikely that the current simulation can provide a reliable model of the background given the experience from the $B_{u,d}^{**}$ analysis and the current lack of knowledge about kaons produced in the fragmentation process.

Although up to three separate peaks in the Q value distribution may be expected, only one peak is observed in data. Therefore, the signal plus background parametrisation

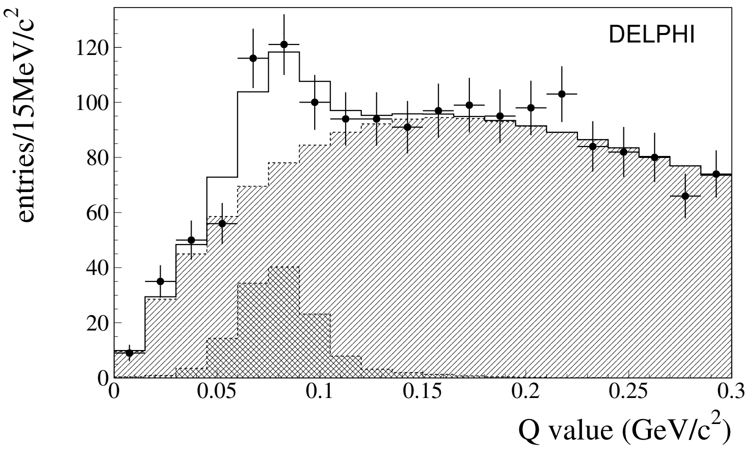

Figure 6: *Result of the fit to the observed Q spectrum in the B_s^{**} analysis. The points are data and the open histogram is the fit result. The hatched histogram shows the background component of the fit and the cross-hatched histogram is assumed to come from the signal contribution.*

is fitted to the measured Q value distribution with the following quantities left free to vary in the fit:

- the signal production rate;
- the signal Q value;
- the four background parameters p_1 to p_4.

The fit is done for different cuts on the B_s^{**} Enhancement Network. An example of the fit to the observed Q spectrum is shown in Figure 6 (corresponding to cut value 2 in Figure 7).

Figure 7 presents results on the B_s^{**} production rate and on the signal Q value, as a function of the cut value on the B_s^{**} Enhancement Network. Different statistical errors are expected when using samples with higher purity, but since both the signal and the background decrease, a nearly constant error is obtained. The results, over a range of purities (from about 19% to 28% as estimated from the simulation), shows that the description of the signal and background components is stable.

Systematic uncertainties on the fit results have been studied by:

- replacing the background model by the shape obtained from the simulation and leaving the normalisation free to vary in the fit;
- varying the Gaussian widths of the signal parametrisation by $\pm$ 10%;
- varying the relative areas of the narrow and broad Gaussian components of the double Gaussian signal fit by $\pm$ 20% and $\mp$ 20% respectively;
- changing the kaon efficiency by -10%.
- varying the energy scale

The uncertainty on the kaon identification efficiency has been obtained by comparing, in data and simulation, kaons from $D^{*+} \to D^0\pi^+$, $D^0 \to K^-\pi^+$. It is found that the efficiency in the simulation is overestimated by at most 10%. This variation resulted in a change in the rate of +0.0011. The production rate has then been shifted by half of this variation and this shift has been assigned as a systematic uncertainty.

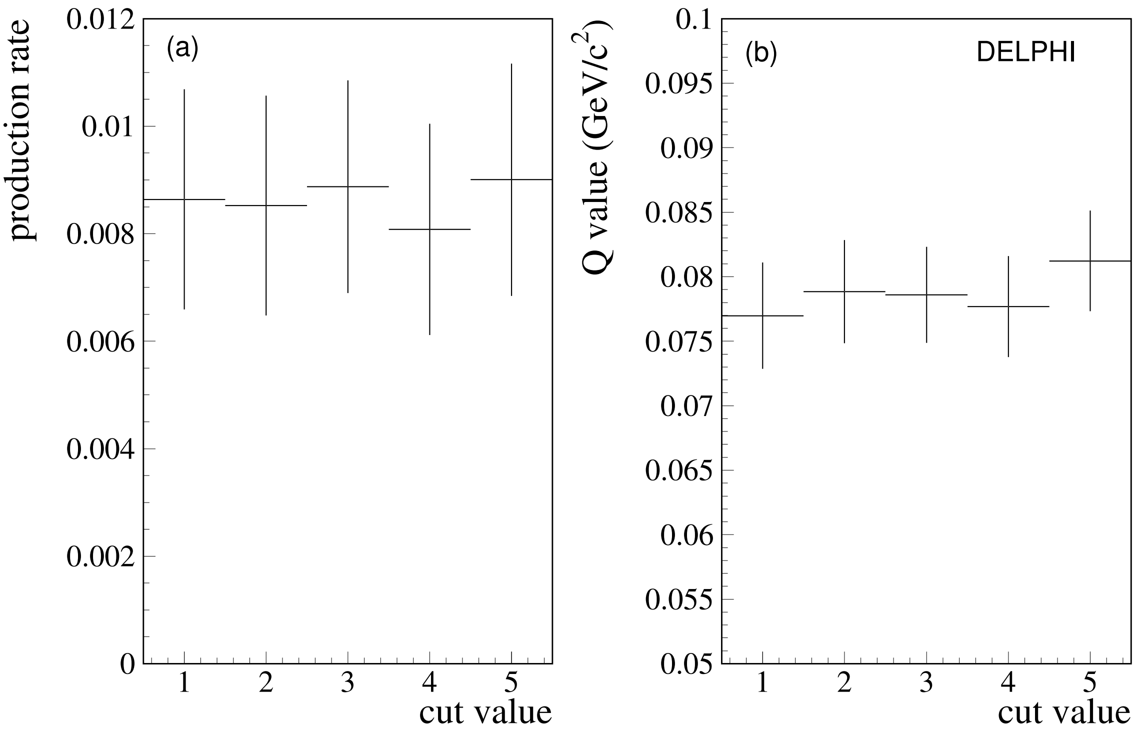

Figure 7: *Results for the* $B^{**}_{\rm rms}$ *(a) signal production rate and (b) signal* Q *value as a function of the cut value on the* B^{**}_s *Enhancement Network. Only statistical errors have been displayed.*

Since the fitted production rates and Q values are stable and have very similar statistical errors as a function of the B^{**}_s purity, the final results are determined by taking the mean of the fit results shown in Figure 7, giving:

$$Q = 79.0 \pm 4.0(\text{stat.}) \pm 3.7(\text{syst.})\ \text{MeV}/c^2$$

$$\frac{\sigma(B^{**}_s)\cdot \text{BR}(B^{**}_s \to \text{BK})}{\sigma_b} = 0.0093 \pm 0.0020(\text{stat.}) \pm 0.0013(\text{syst.}).$$

The fit result on the production rate and its uncertainties have been multiplied by a factor two to account for the unmeasured decay into B^0K^0.

The breakdown of the systematic uncertainties is given in Table 14. The significance of the reconstructed signal is 3.8σ including systematics.

It is possible to extract from the fit a limit on the width of the narrow B^{**}_s state observed. This was done by allowing for additional width of the signal. The signal is compatible with an infinitely narrow width. The upper limit on the width corresponds to 13 MeV/c^2 at 95% C.L. including systematic errors.

Interpretation of the observed signal

As discussed in Section 4.2, two (or three) peaks from narrow B^{**}_s states are expected. If the signal is interpreted as originating from $B_{s1} \to B^*K$ decays, a signal from the decay $B^*_{s2} \to BK$ at a Q value around 140 MeV/c^2 is expected. The precise Q value depends

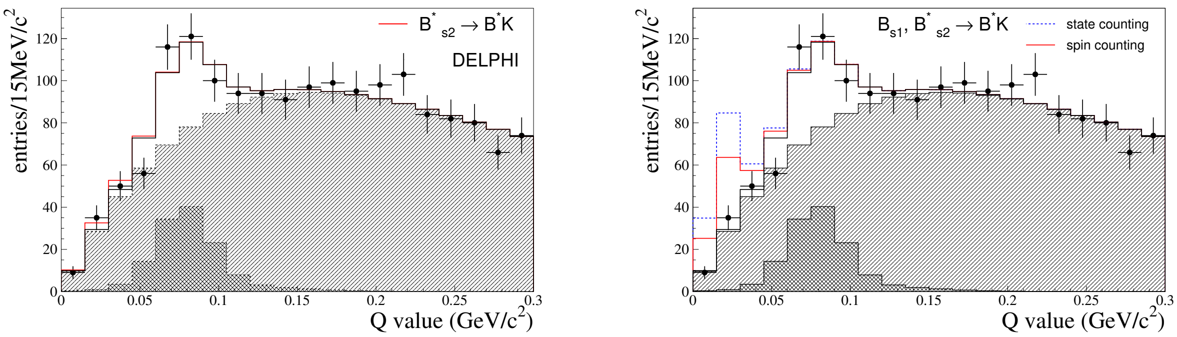

Figure 8: *The main signal is assumed to come from* $\mathrm{B}^*_{\mathrm{s}2} \to \mathrm{BK}$. *In the plot on the left, expected contributions from* $\mathrm{B}^*_{\mathrm{s}2} \to \mathrm{B}^*\mathrm{K}$ *have been added. They correspond to a small amount of events situated on the left of the main signal. The resulting spectrum is compatible with present measurements. In the plot on the right, the possible decay* $\mathrm{B}_{\mathrm{s}1} \to \mathrm{B}^*\mathrm{K}$ *has been added, for the scenarios of spin and state-counting. The resulting spectrum is not compatible with present measurements implying that the* $\mathrm{B}_{\mathrm{s}1}$ *state decays mainly through unseen decay modes as, for instance, those involving* $\mathrm{B}_{\mathrm{s}}^{(*)}$ *mesons. Only statistical errors are shown.*

on the $\mathrm{B}^*_{\mathrm{s}2} - \mathrm{B}_{\mathrm{s}1}$ mass splitting. This peak should clearly be visible in the data as the reconstruction efficiency increases as a function of the Q value. This interpretation is therefore not supported by the data.

If the signal comes from $\mathrm{B}^*_{\mathrm{s}2} \to \mathrm{BK}$ decays, the decay mode $\mathrm{B}^*_{\mathrm{s}2} \to \mathrm{B}^*\mathrm{K}$ should be seen at a Q value of about 33 MeV/c^2. But the latter is expected to be suppressed by a factor 1/10 as compared to the former (see Section: 2.2.2). This interpretation, shown in Figure 8-left, gives a reasonable description of the data.

However, the question remains, where the signal from the decay $\mathrm{B}_{\mathrm{s}1} \to \mathrm{B}^*\mathrm{K}$ is. A signal at Q values lower than 79-46=33 MeV/c^2 is expected. If a mass splitting of 13 MeV/c^2 is assumed, a peak at a Q value of 20 MeV/^{2} should be observable. The reconstruction efficiency is reduced by 65% at this Q value. This scenario is illustrated for the hypothesis

Systematic source	Uncertainty in Q	Uncertainty in rate
	MeV/c^2	
Background shape	1.8	0.0008
Signal width	+0.2	+0.0006
Signal area	+0.3	−0.0005
Kaon efficiency	-	0.0006
Energy scale	3.2	-
Total	3.7	0.0013

Table 14: *Systematic errors on the measured* Q *value and on the production rate for* $\mathrm{B}_{\mathrm{s}}^{**}$ *mesons. The signs refer to the direction of the change induced by an upwards variation in the error source.*

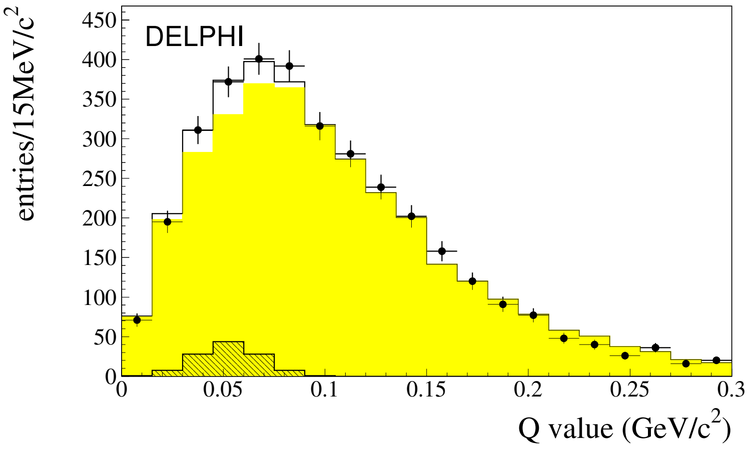

Figure 9: *The Q distribution used to extract the upper limit on the production of $\Sigma_b^{(*)}$ baryons. The points are data and the open histogram is the fit result. The hatched histogram shows the fitted background and the cross-hatched histogram the fitted Gaussian.*

of state and spin-counting in Figure 8-right. This scenario is not favoured by the data. However it might be argued that the isospin forbidden decay $\mathrm{B_{s1}} \to \mathrm{B_s^*}\pi^0$ is enhanced over the allowed decay mode near threshold. The variation of the decay rate in proportion to the fifth power of the internal momentum provides more than two orders of magnitude enhancement for the isospin-forbidden decay. Electromagnetic transitions of the $\mathrm{B_{s1}}$ state may also have a non-negligible contribution. These effects would effectively reduce the $\mathrm{B_{s1}} \to \mathrm{B^*K}$ signal.

The broad $\mathrm{B_s^{**}}$ states could lie below threshold, as recent results in the charm sector seem to indicate. If broad $\mathrm{B_s^{**}}$ states are above threshold, it is likely that they are absorbed in the fitted background.

For these reasons, the most probable interpretation is that the observed signal comes from the decay $\mathrm{B_{s2}^*} \to \mathrm{BK}$. In this case, the measured Q value corresponds to a mass of $m(\mathrm{B_{s2}^*}) = 5852 \pm 5$ MeV/c^2. The upper limit on the intrinsic width of the $\mathrm{B_{s2}^*}$ state is 13 MeV/c^2 at 95% C.L. A limit on the ratio of the branching fractions including systematic errors can be extracted for this interpretation by fitting another narrow resonance at the expected Q value with the same procedure used for the previous fit:

$$\frac{\sigma(\mathrm{B_{s1}}) \cdot \mathrm{BR}(\mathrm{B_{s1}} \to \mathrm{B^*K})}{\sigma(\mathrm{B_{s2}^*}) \cdot \mathrm{BR}(\mathrm{B_{s2}^*} \to \mathrm{BK})} \quad < \quad 0.40 \text{ @ } 95\%\text{C.L.}$$

which translates into a limit of the $\mathrm{B_{s1}}$ production rate of:

$$\frac{\sigma(\mathrm{B_{s1}}) \cdot \mathrm{BR}(\mathrm{B_{s1}} \to \mathrm{B^*K})}{\sigma_\mathrm{b}} \quad < \quad 0.0040 \text{ @ } 95\%\text{C.L.}$$

7 A Search for $\Sigma_b^{(*)}$ Baryons

A search for $\Sigma_b^{(*)}$ baryons, in the decay channel $\Lambda_b\pi^\pm$, has been made using the HPA approach. Events are reconstructed using a dedicated neural network to select charged pions coming from a $\Sigma_b^{\pm(*)}$ decay. The final state Λ_b baryon is identified by a neural network [31] similar to the B^+-Net and B^0-Net. The signal is described by a single Gaussian with a width fixed to the expected resolution, the background is parametrised using the expression given in Equation (9) which contains four free parameters a, b, c and d.

No narrow signal is observed in data, shown in Figure 9, in the Q value range smaller than 0.2 GeV/c^2. The measured Q distribution is fitted to determine the following upper limit on the production rate of a single narrow Σ_b or Σ_b^* resonance[3] at 95% C.L.:

$$\frac{\sigma(\Sigma_b^{(*)}) \cdot \mathrm{BR}(\Sigma_b^{(*)} \to \Lambda_b \pi)}{\sigma_b} = \frac{1}{\sigma_b} \sum_{i=+,0,-} \sigma(\Sigma_b^{(*)i}) \cdot \mathrm{BR}(\Sigma_b^{(*)i} \to \Lambda_b \pi^i)$$

$$\frac{\sigma(\Sigma_b^{(*)}) \cdot \mathrm{BR}(\Sigma_b^{(*)} \to \Lambda_b \pi)}{\sigma_b} < 0.012$$

in the Q value range smaller than 0.2 GeV/c^2. This limit has been scaled by a factor 3/2 to account for unseen channels, namely $\Sigma_b^{(*)0} \to \Lambda_b \pi^0$.

The upper limit includes the systematic uncertainty coming from variations in the Σ_b purity and uncertainty in the background parametrisation. The fit result used to extract this limit is shown in Figure 9.

8 Summary and Conclusion

New analyses on excited b-hadron states have been presented. For $B^{**}_{u,d}$ mesons, the results of the High Efficiency and High Purity Analyses have been combined to give a total $B^{**}_{u,d}$ production rate of

$$\frac{\sigma(B^{**}_{u,d}) \cdot \mathrm{BR}(B^{**}_{u,d} \to B^{(*)}\pi)}{\sigma_b} = 0.156 \pm 0.011(\mathrm{stat.})^{+0.022}_{-0.014}(\mathrm{syst.}) \pm 0.019(\mathrm{model}).$$

The narrow $B^{**}_{u,d}$ production rate has been determined to be

$$\left(\frac{\sigma(B^{**}_{u,d}) \cdot \mathrm{BR}(B^{**}_{u,d} \to B^{(*)}\pi)}{\sigma_b}\right)_{\mathrm{narrow}} = 0.091 \pm 0.007(\mathrm{stat.})^{+0.013}_{-0.008}(\mathrm{syst.}) \pm 0.011(\mathrm{model}).$$

These measurements have high statistical accuracy and reduced systematics as compared with previous analyses (see Table 4) because of an experimental control of the combinatorial background. The mass of the B_2^* meson has been measured:

$$m(B_2^*) = 5738 \pm 14 \ \mathrm{MeV/c}^2$$

and the mass splitting between the two narrow states B_2^* and B_1 has been determined to be:

$$m(B_2^*) - m(B_1) = 6 \pm 11(\mathrm{stat.}) \pm 7(\mathrm{syst.}) \pm 6(\mathrm{model}) \ \mathrm{MeV/c}^2,$$

leading to a B_1 mass of:

$$m(B_1) = 5732 \pm 20 \ \mathrm{MeV/c}^2.$$

These results supersede those previously published by DELPHI [20].

[3] The upper limit on the production rate corresponds to the production of a single Σ_b or Σ_b^* state, not to their sum.

For $\mathrm{B}_{\mathrm{s}}^{**}$ mesons, only one peak in the Q distribution could be observed which is interpreted as originating from the decay $\mathrm{B}_{s2}^{*} \rightarrow \mathrm{BK}$. The production rate has been measured to be:

$$\frac{\sigma(\mathrm{B}_{\mathrm{s2}}^{*}) \cdot \mathrm{BR}(\mathrm{B}_{\mathrm{s2}}^{*} \rightarrow \mathrm{BK})}{\sigma_{\mathrm{b}}} = 0.0093 \pm 0.0020(\mathrm{stat.}) \pm 0.0013(\mathrm{syst.})$$

and the B_{s2}^{*} mass has been extracted:

$$m(\mathrm{B}_{s2}^{*}) = 5852 \pm 5 \ \mathrm{MeV/c}^{2}.$$

All measured narrow $\mathrm{B}_{\mathrm{u,d,s}}^{**}$ signals have a width which is compatible with the experimental resolution[4].

No narrow signal is observed for $\Sigma_{\mathrm{b}}^{(*)}$ baryons. An upper limit on the production rate of a narrow resonance of

$$\frac{\sigma(\Sigma_{\mathrm{b}}^{(*)}) \cdot \mathrm{BR}(\Sigma_{\mathrm{b}}^{(*)} \rightarrow \Lambda_{\mathrm{b}}\pi)}{\sigma_{\mathrm{b}}} < 0.012 \ @ \ 95\% \ \mathrm{C.L.}$$

has been extracted in the Q value range smaller than 0.2 $\mathrm{GeV/c}^{2}$.

[4] In PDG2004 [13], an intrinsic width of $128 \pm 18\mathrm{MeV/c}^{2}$ is quoted for $\mathrm{B}_{\mathrm{u,d}}^{**}$ mesons. It corresponds to an average over narrow and broad states.

References

[1] N. Isgur, M. B. Wise, Phys. Lett. **B232** (1989) 113;
N. Isgur, M. B. Wise, Phys. Lett. **B237** (1990) 527;
M. B. Wise: 'Heavy Flavor Theory: Overview'. In: Proceedings of the 16th International Symposium on Lepton and Photon Interactions, 1993, Ithaca, NY, pp 253-273, ed by P. Drell, D. Rubin, AIP Conference Proceedings 302, hep-ph/9311212;
N. Isgur, M. B. Wise: 'Heavy Quark Symmetry'. In: *B Decays*, 2nd edition, ed. S. Stone (World Scientific, 1994), 231;
M. Neubert: 'B Decays and the Heavy-Quark Expansion'. In: *Heavy Flavours II*, Advanced Series on Directions in High Energy Physics - Vol. 15, ed by A. J. Buras, M. Lindner (World Scientific, 1998), 239 hep-ph/9702375.

[2] S. Godfrey and N. Isgur, Phys. Rev **D32** (1985) 189.

[3] S. Godfrey and R. Kokoski, Phys. Rev. **D43** (1991) 1679.

[4] M. Gronau and J. L. Rosner, Phys. Rev. **D49** (1994) 254.

[5] S. N. Gupta and J. M. Johnson, Phys. Rev. **D51** (1995) 168.

[6] N. Isgur, Phys. Rev. **D57** (1998) 4041.

[7] D. Ebert, V. O. Galkin and R. N. Faustov, Phys. Rev. **D57** (1998) 5663;
Erratum-ibid. **D 59** (1999) 019902.

[8] A. F. Falk, M. E. Peskin, Phys. Rev. **D49** (1994) 3320.

[9] A. F. Falk and T. Mehen, Phys. Rev. **D53** (1996) 231.

[10] E. J. Eichten, C. T. Hill and C. Quigg, Phys. Rev. Lett. **71** (1993) 4116;
E. J. Eichten, C. T. Hill and C. Quigg, Fermilab Conf 94/118 T.

[11] A. H. Orsland and H. Hogaasen, Eur. Phys. J. **C9** (1999) 503 .

[12] M. DiPierro and E. Eichten, Phys. Rev. **D64** (2001) 114004 .

[13] Particle Data Group, S. Eidelman et al., Phys. Lett. **B592** (2004) 1.

[14] CLEO Collab., S. Anderson et al., Nucl. Phys. **A663** (2000) 647.

[15] BELLE Collab., K. Abe et al., Phys. Rev. **D69** (2004) 112002.

[16] BABAR Collab., B. Aubert et al., Phys. Rev. Lett. **90** (2003) 242001;
CLEO Collab., D. Besson et al., Phys. Rev. **D68** (2003) 032002.

[17] CLEO Collab., T. Bergfeld et al., Phys. Lett. **B340** (1994) 194.

[18] CLEO Collab., Y. Kubota et al., Phys. Rev. Lett. **72** (1994) 1972.

[19] OPAL Collab., R. Akers et al., Z. Phys. **C66** (1995) 19.

[20] DELPHI Collab., P. Abreu et al., Phys. Lett. **B345** (1995) 598.

[21] ALEPH Collab., D. Buskulic et al., Z. Phys. **C69** (1996) 393;

[22] ALEPH Collab., R. Barate et al., Phys. Lett. **B425** (1998) 215.

[23] L3 Collab., M. Acciarri et al., Phys. Lett. **B465** (1999) 323.

[24] OPAL Collab., G. Abbiendi et al., Euro Phys. J. **C23** (2002) 437.

[25] CDF Collab., T. Affolder et al., Phys. Rev. **D64** (2001) 072002.

[26] DELPHI Collab., P. Aarnio et al., Nucl. Instr. and Meth. **A303** (1991) 233;

[27] DELPHI Collab., P. Abreu et al., Nucl. Instr. and Meth. **A378** (1996) 57.

[28] DELPHI Collab., J. Abdallah et al., Eur. Phys. J. **C28** (2003) 155.

[29] T. Sjöstrand, Computer Phys. Comm. **39** (1986) 347;
T. Sjöstrand and M. Bengtsson, Computer Phys. Comm. **43** (1987) 367.

[30] DELPHI Collaboration, P. Abreu et al., Z. Phys. **C73** (1996) 11.

[31] Z. Albrecht et al., *BSAURUS-A Package For Inclusive B-Reconstruction in DELPHI*, hep-ex/0102001.

[32] Z. Albrecht, M. Feindt, M. Moch, *MACRIB, High Efficiency, High Purity Hadron Identification for DELPHI*, hep-ex/0111081.

[33] DELPHI Collab., J. Abdallah et al., Eur. Phys. J. **C33** (2004) 307.
[34] DELPHI Collab., J. Abdallah et al., Eur. Phys. J. **C40** (2005) 1.
[35] DELPHI Collaboration, J. Abdallah et al., Eur. Phys. J. **C32** (2004) 185.
[36] DELPHI Collab., P. Abreu et al., Phys. Lett. **B475** (2000) 429.
[37] M. Feindt, *A Neural Bayesian Estimator for Conditional Probability Densities*, physics/0402093.